Supporting information

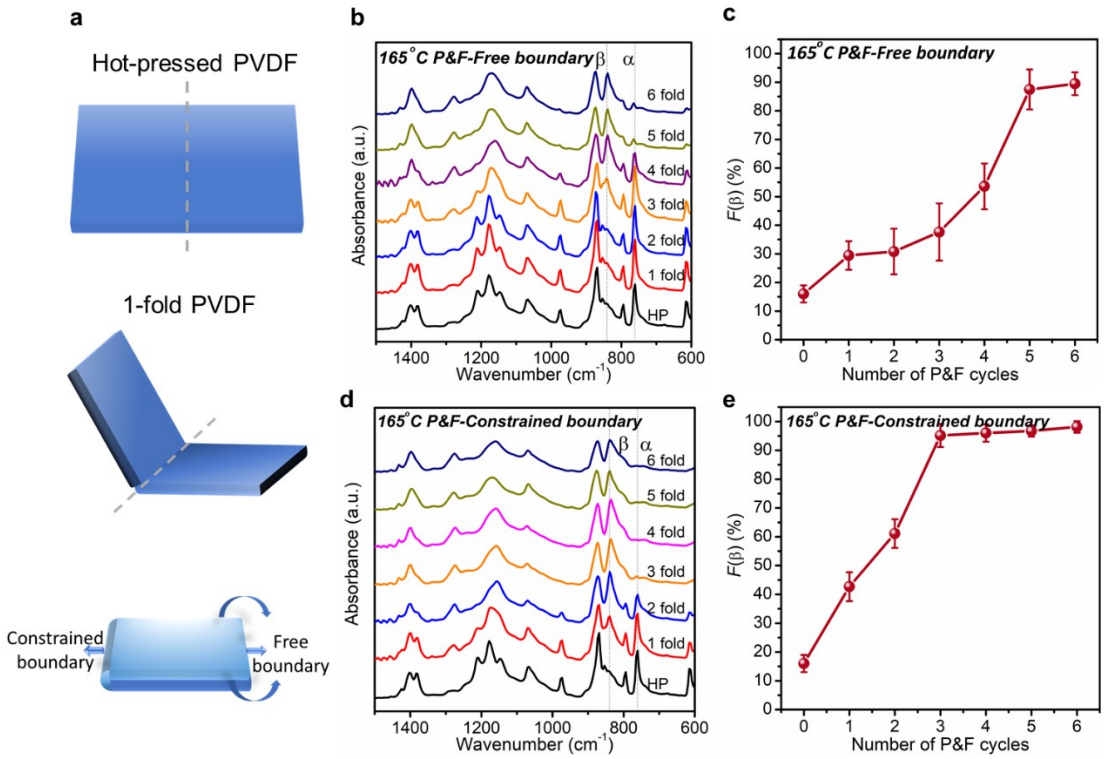

Figure S1. Comparison of α- to β- phase transformation folded boundaries and free boundaries of "Press & Fold" (P&F) PVDF prepared at 165 °C. For further experimental details, refer to the previous papers.[1, 2] **a**, Schematic diagram of "fold", which produced different boundary conditions: folded with free boundaries During each fold, 4 boundaries were generated, including 3 free boundaries and 1 folded boundary. All of the measurements were conducted close to the boundaries (within approximately 3 mm). 10 measurements were performed to reveal the homogeneity of the film. (**b** and **d**), FTIR spectra; (**c** and **e**), $F(\beta)$ of PVDF P&F from 0 to 6 cycles for the "folded boundary" and "free boundary", respectively. From 1 to 4 P&F cycles, the "folded boundary" part of the film displayed higher β-phase content compared with the "free boundary" part for the same P&F cycle, suggesting the folded boundaries are more effective than "free boundary" in terms of phase transformation.

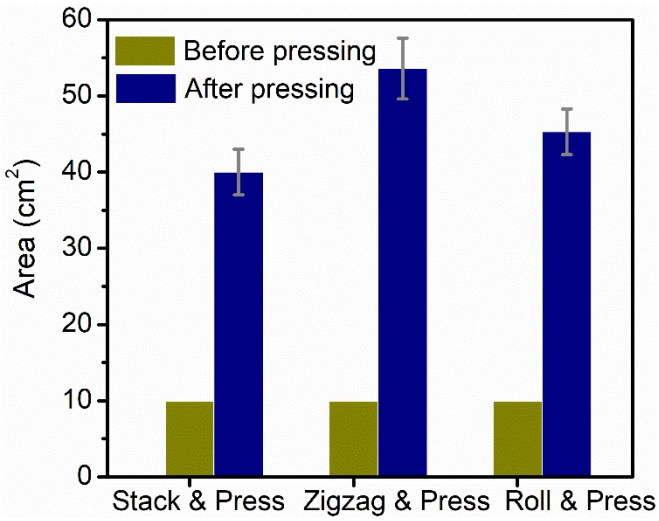

Figure S2. The measured area of multilayer PVDF with different boundary conditions before and after pressing. The larger area changes in Roll & Press and Zigzag & Press suggest folded boundaries are favourable for the stress transfer and enhance the local stress during pressing.

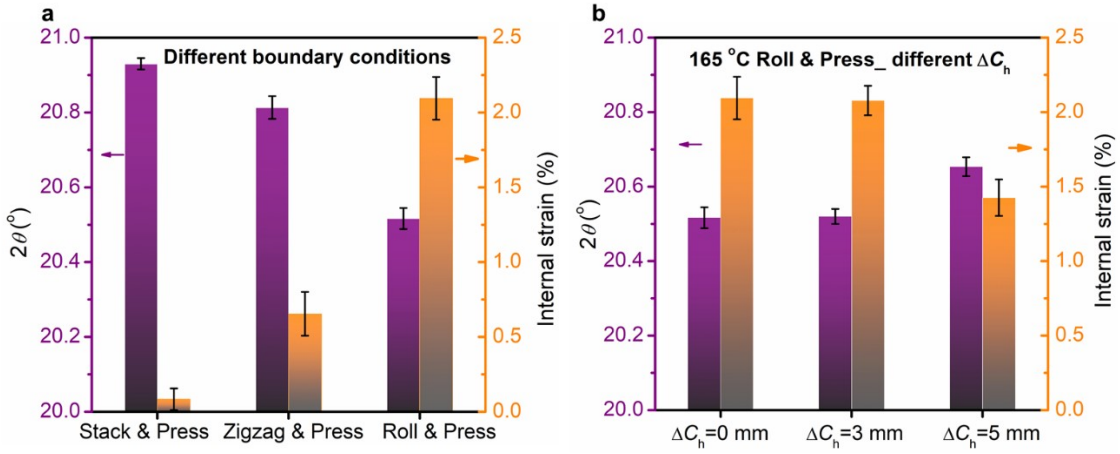

Figure S3. Comparison of $(110/200)_\beta$ diffraction peak position 2θ and estimated internal strain: **a**, PVDF films with different boundary conditions including Stack & Press, Zigzag & Press and Roll & Press; **b**, Roll & Press PVDF films with ΔC_h of 0, 3 mm and 5 mm.

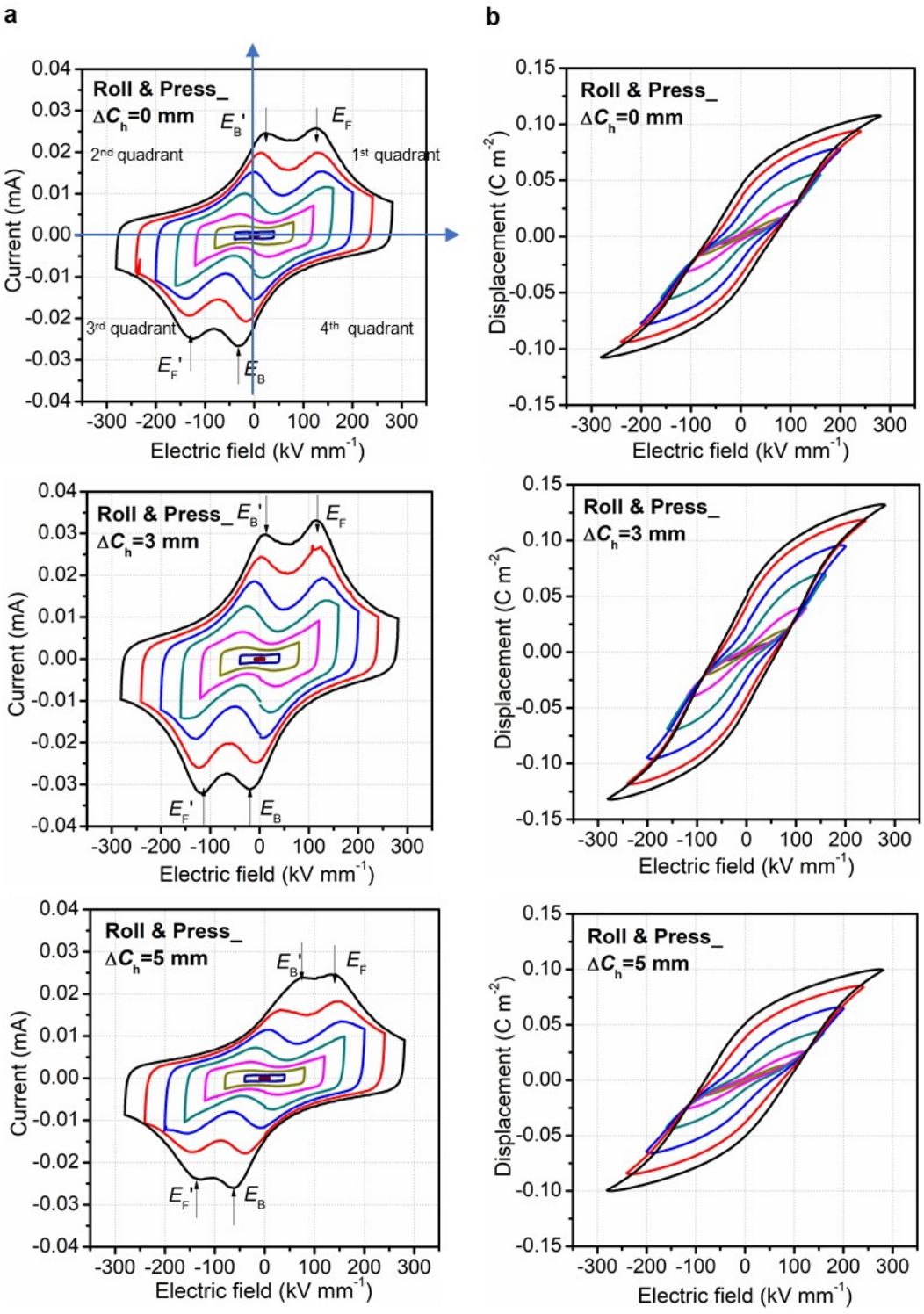

Figure S4. a, *I-E*; **b**, *D-E* loops of Roll & Press films with ΔC_h of 0, 3 mm and 5 mm.

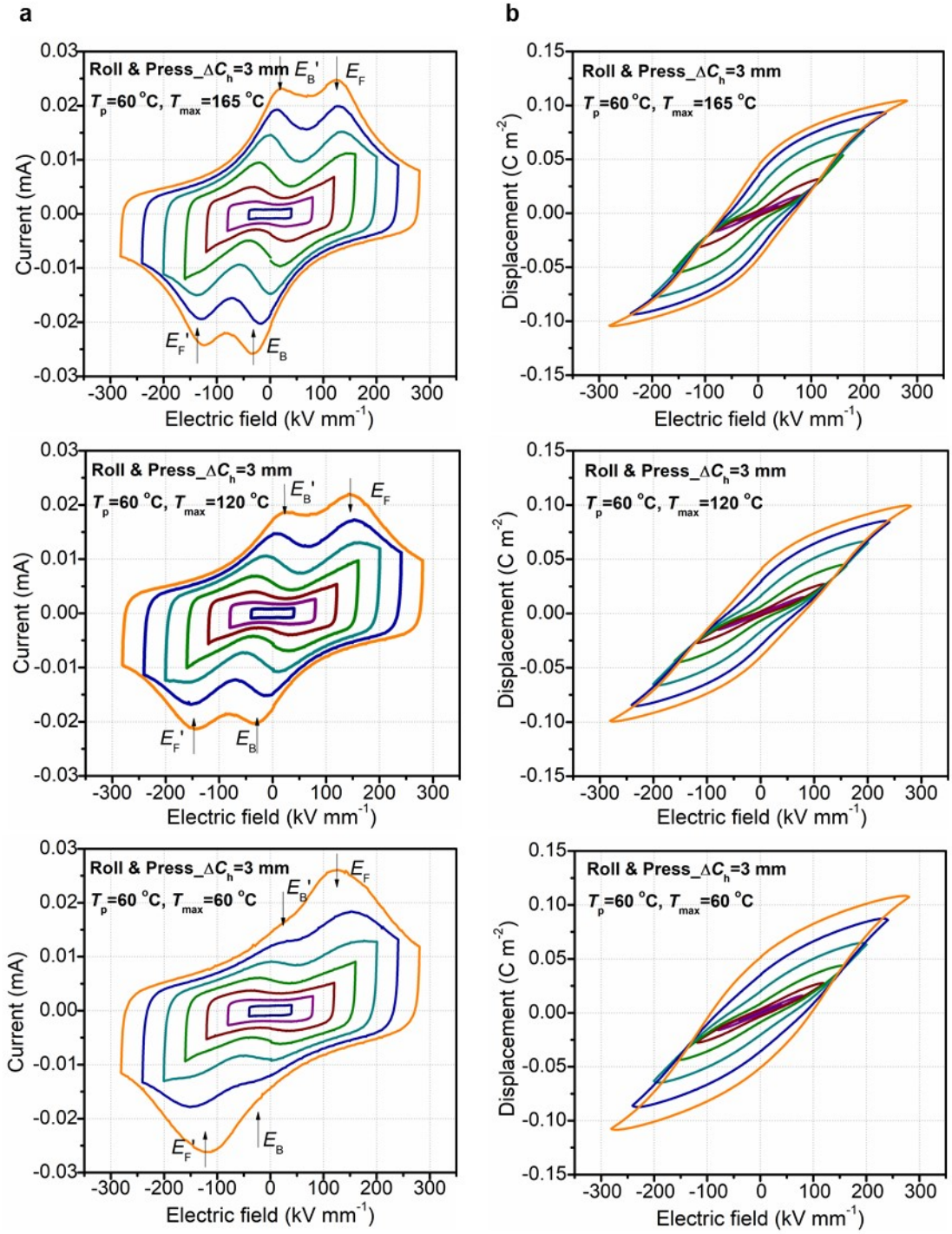

Figure S5. a, *I-E*; **b**, *D-E* loops of Roll & Press films with ΔC_h of 3mm and at T_{max} of 60 °C, 120 °C, 165 °C. Among this group of Roll & Press films, none of them showed stable relaxor-like ferroelectric behaviour. The reason is none of these films exhibited both high $F(\beta)$ and high internal strain. For the Roll & Press film prepared at T_p of 60 °C and T_{max} of 165 °C, although the $F(\beta)$ reached 90 % (FTIR), the internal strain was only 2.1 %. The internal strain increased to 4.3 % in film prepared at T_p of 60 °C and T_{max} of 60 °C, but the $F(\beta)$ decreased to 59 % (FTIR).

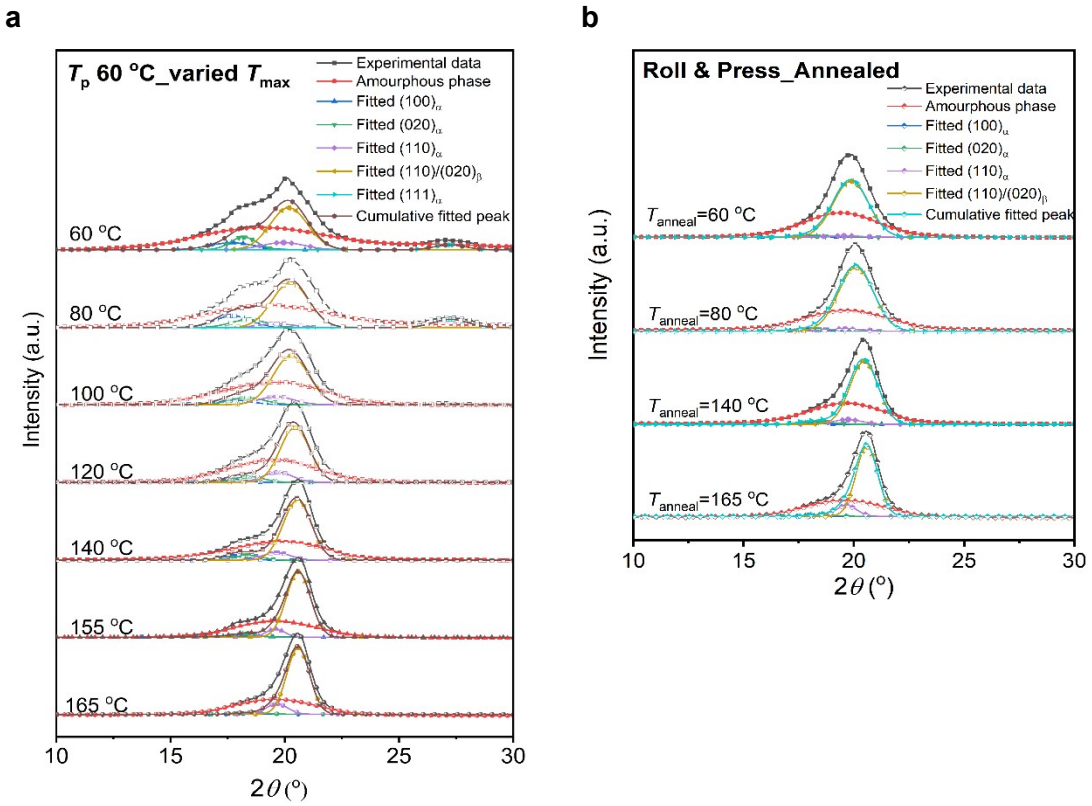

Figure S6. Deconvoluted XRD patterns for: **a**, Roll & Press PVDF film with ΔC_h of 3 mm prepared at a constant T_p of 60 °C with T_{max} varying from 165 °C to 60 °C; **b**, Roll & Press PVDF films with ΔC_h of 3mm prepared at T_p of 60 °C and T_{max} of 165 °C, followed by annealing at 165 °C, 140 °C, 80 °C and 60 °C. All the Gaussian-fitted results reached a coefficient of determination (R^2) of 99.5 % relating to the experimental data.

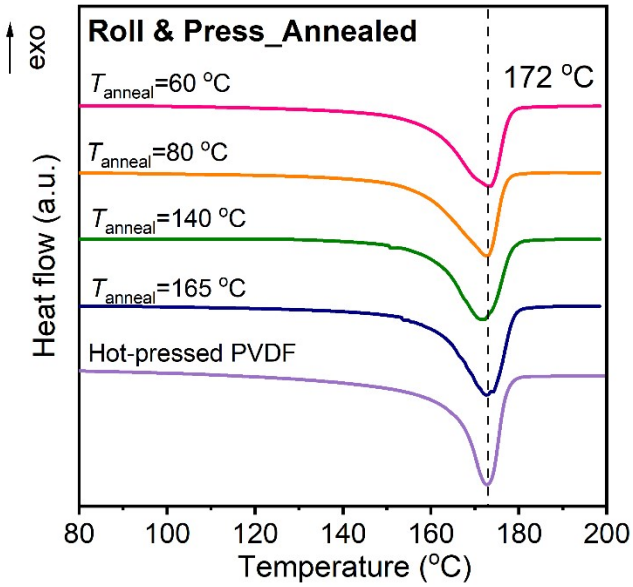

Figure S7. Comparison of DSC 1st heating curves for hot-pressed PVDF film and Roll & Press PVDF films with ΔC_h of 3 mm prepared at T_p of 60 °C and T_{max} of 165 °C, followed by annealing at 165 °C, 140 °C, 80 °C and 60 °C.

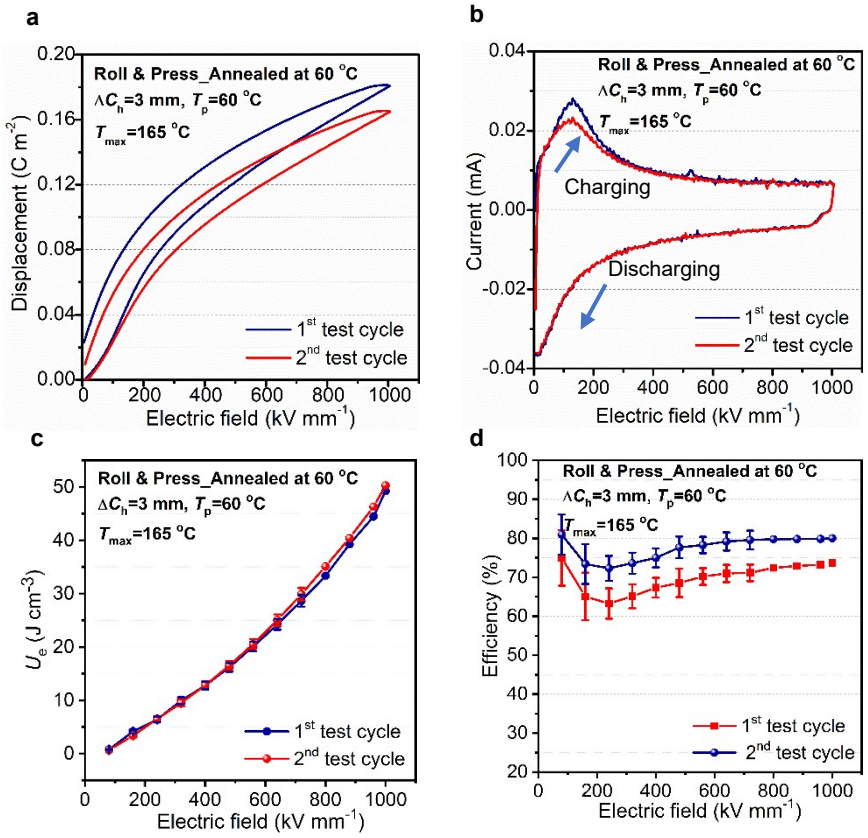

Figure S8. Ferroelectric properties of the 60 °C annealed Roll & Press film with ΔC_h of 3 mm at high electric field were measured using two consecutive half-cycle (denoted as 1st and 2nd) triangular waveforms at 10 Hz: **a**, 1st cycle unipolar *D-E* loops; **b**, Comparison of *I-E* loops at 1000 kV mm^{-1}; **c**, U_e; **d**, η from 80 to 1000 kV mm^{-1} for both 1st and 2nd cycles. During the first charging cycle, both reversible polar nanostructures and irreversible field-induced ferroelectric domains (originating from the small amount of α-β phase transition) contributed to the maximum electric field induced displacement $D_{\text{in-max}}$. As a result, higher D_{in} and D_{r} were observed in the 1st cycles *D-E* loops compared with the 2nd cycles (Figure 3c) at the same electric field. During the first discharging cycle, the reversible polar structure mainly contributed to the discharged energy density because most of the ferroelectric domains cannot switch back to their original state, which results in high energy loss. When the test was repeated at the same electric field for more cycles, the charge-discharge efficiency gradually increased because some of the field induced and aligned ferroelectric domains tended to become inactive (also shown in Figure S14). This is confirmed by reduced peak intensity in the *I-E* loop for the 2nd test cycle during charging. Therefore, the η increased from 74 % to 80 % at 1000 kV mm^{-1} during 2nd cycle, as a result of the suppressed irreversible polarisation. Therefore, during the repetitive operations of the Roll & Press PVDF under high fields, the energy storage efficiency is higher than the value measured during the first charge-discharge cycle, which is desirable considering the long service life of dielectric capacitors.

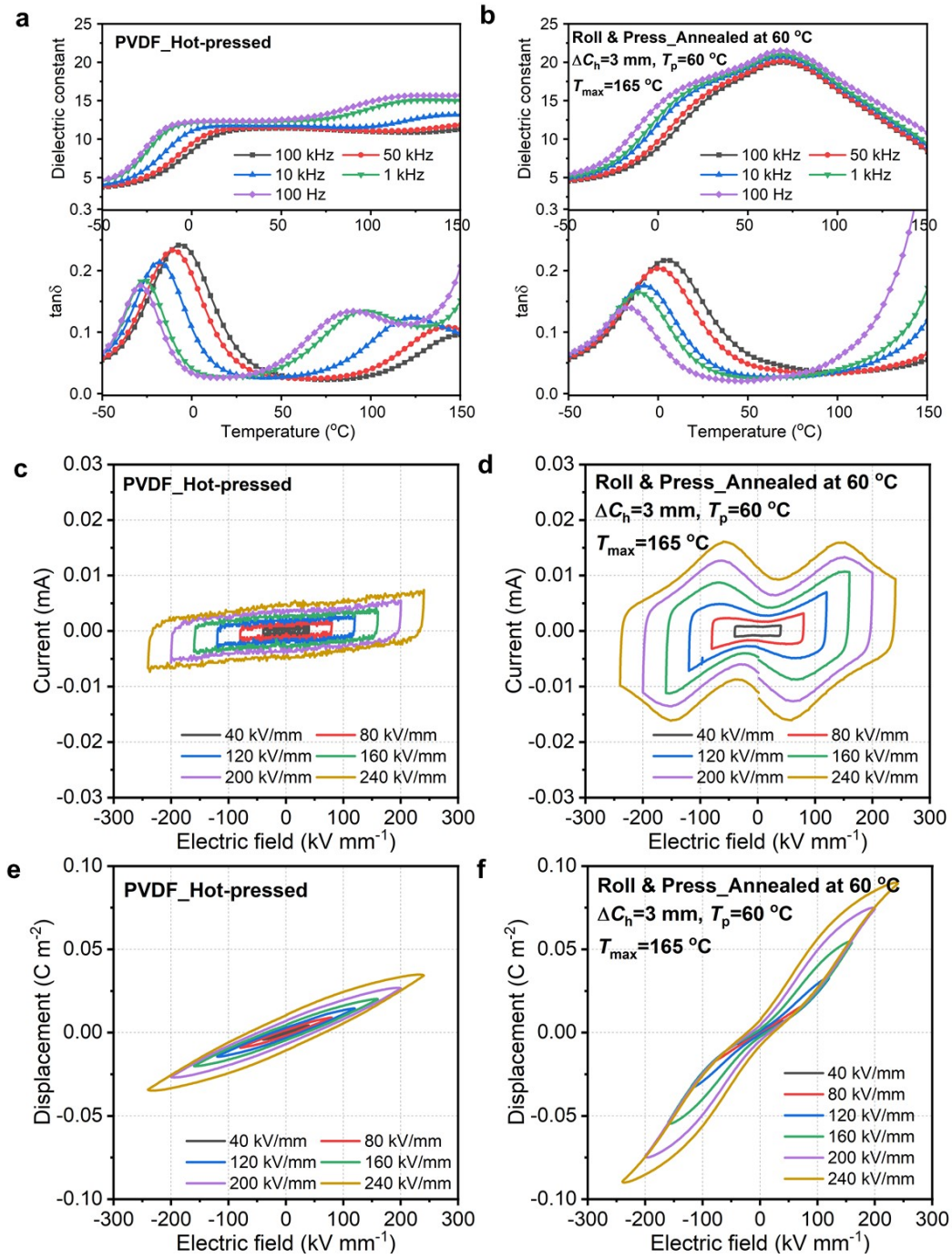

Figure S9. Comparison of dielectric and ferroelectric properties for hot-pressed PVDF film and 60 °C annealed Roll & Press PVDF film with ΔC_h of 3 mm: **a** and **b**, temperature dependent dielectric constant/loss spectra; **c** and **d**, *I-E* loops from 40 to 240 kV mm^{-1}; **e** and **f**, *D-E* loops from 40 to 240 kV mm^{-1}. The comparison was done at 240 kV mm^{-1} due to the limit of high voltage power supply (maximum: 10 kV) and the practical difficulty in achieving thin hot-pressed PVDF film (< 40 μm) because of the polymer's high viscosity. The Roll & Press PVDF film exhibited enhanced properties in both low-field dielectric constant (ε_r) and high-field induced displacement (D_{in}). A remarkable change was found in the **a** and **b**, where the high temperature α_c relaxation (75 - 150 °C) observed in the hot-pressed PVDF was replaced by a

broad frequency-independent peak around 73 °C with a higher ε_r of 20.5 in Roll & Press PVDF film, indicating the thermal energy enhanced the mobility of dipoles in the Roll & Press PVDF film. The dipole mobility reached the maximum at ~ 73 °C and then started decreasing afterwards.

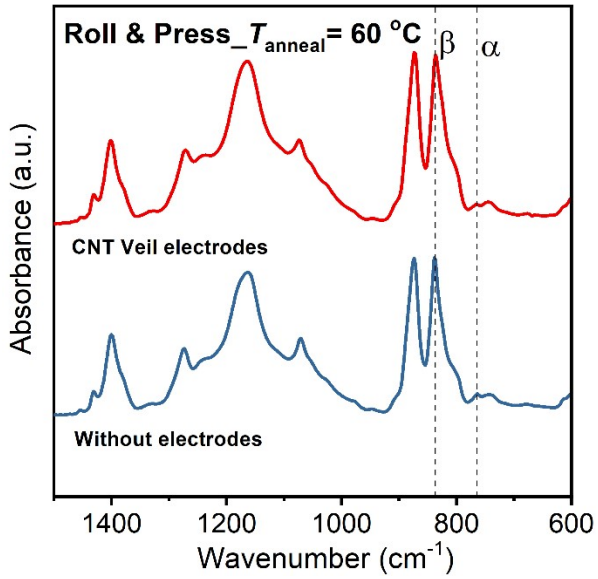

Figure S10. FTIR spectra of the assembled capacitor with CNT Veil electrodes (T_p = 60 °C, T_{max} = 165 °C, T_{anneal} = 60 °C) and its corresponding neat Roll & Press PVDF film under the same conditions. The calculated $F(\beta)$ for the above two films are 95 ± 2 % and 94 ± 3 %, respectively. These results demonstrate that adding the conductive CNT Veil layer did not affect the phase transformation during Roll & Press.

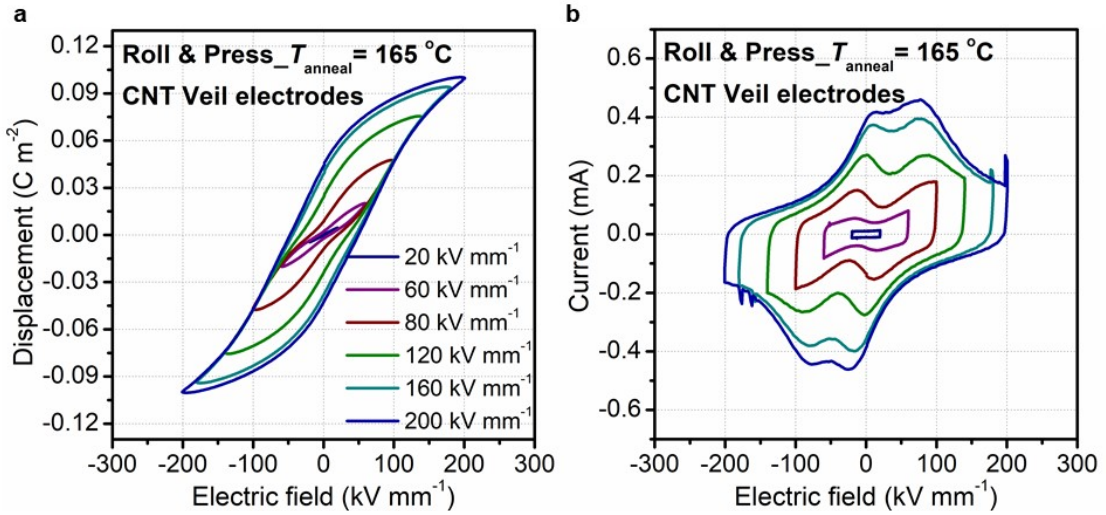

Figure S11. a, *I-E*; **b**, *D-E* loops up to 200 kV mm^{-1} for the assembled capacitor with CNT Veil electrodes (T_p = 60 °C, T_{max} = 165 °C) followed by annealing at 165 °C. As revealed by the emerging current peaks (E_B and E_F', E_B' and E_F), and high D_r, the reversible polar nanostructure is not stable at high fields.

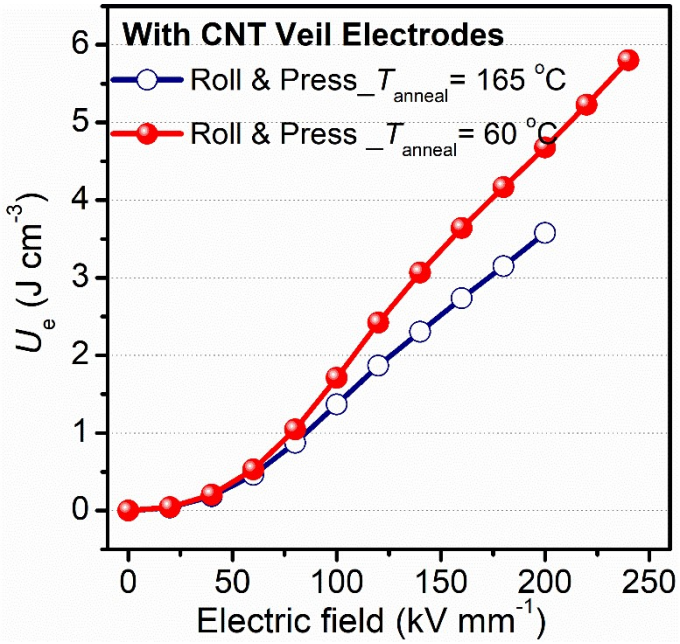

Figure S12. Comparison of discharged energy density U_e for the assembled capacitor prepared with annealing at 165 and 60 °C.

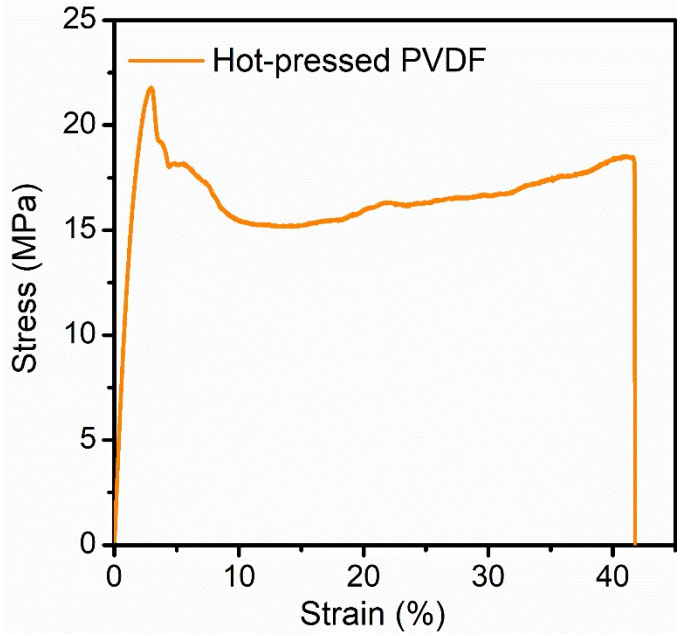

Figure S13. Tensile stress-strain curve of hot-pressed PVDF film.

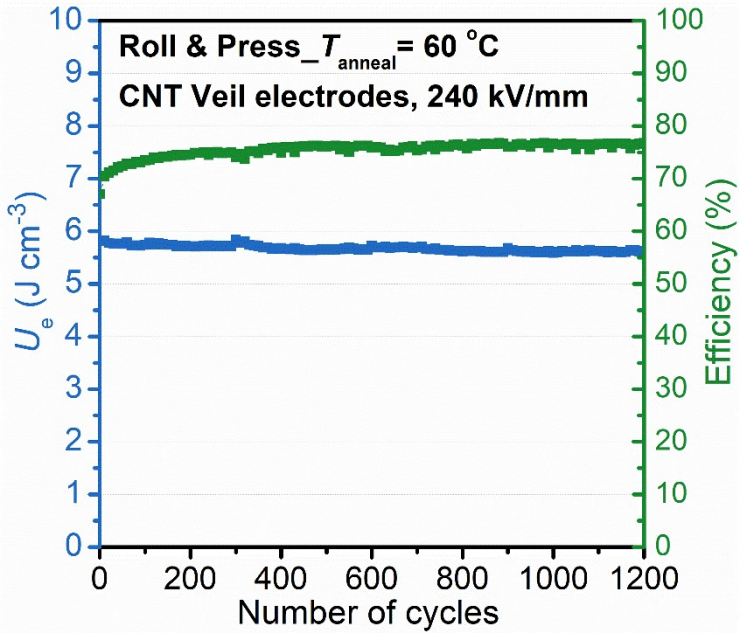

Figure S14. Discharged energy density (U_e) and charge-discharge efficiency of Roll & Press PVDF/CNT veil device over 1200 cycles of *D-I-E* tests. To evaluate the long-term energy storage performance of the PVDF/CNT veil device under the fast charge-discharge operation condition, unipolar *D-I-E* loop measurement was repeated 1200 times using the same sample at room temperature, 240 kV mm^{-1}, and 10 Hz. Due to the data storage limitation of the software for each file (maximum 30 data sets), the repetitive *D-I-E* loops recorded every 10 cycles, and 120 sets of data were obtained to show the performance trend. Based on the experiment results, the U_e is stable over the whole test period (5.67 ± 0.05 J cm^{-3}). The charge-discharge efficiency experienced an increase from 66.2 % to 75.8 % during the first 400 cycles and then stabilised hereafter. The average efficiency over the whole test period is 75.4 ± 1.6 % ascribing to the stabilised polar nanostructures at high electric fields. Overall, the device demonstrated stable energy storage performance during long-term repetitive charge-discharge process.

Table S1. Comparison of crystalline phase compositions and relevant parameters for Roll & Press PVDF with ΔC_h of 3 mm at T_p of 60 °C and T_{max} from 165 to 60 °C.

T_{max} (°C)	T_{anneal} (°C)	Phase composition		$(110/200)_\beta$		
		$F(\alpha)$ (%)	$F(\beta)$ (%)	Peak position (°)	Internal strain (%)	crystallite size (nm)
165	165	15	85	20.55 ± 0.03	2.1 ± 0.2	6.3 ± 0.2
155	155	17	83	20.56 ± 0.02	2.1 ± 0.1	6.2 ± 0.2
140	140	20	80	20.49 ± 0.04	2.4 ± 0.2	5.3 ± 0.2
120	120	17	83	20.39 ± 0.02	2.8 ± 0.1	4.6 ± 0.1
100	100	23	77	20.25 ± 0.03	3.5 ± 0.2	4.1 ± 0.2
80	80	32	68	20.20 ± 0.03	3.8 ± 0.2	4.0 ± 0.2
60	60	34	66	20.12 ± 0.04	4.3 ± 0.1	3.8 ± 0.2
165	140	14	86	20.43 ± 0.02	2.6 ± 0.2	5.0 ± 0.3
165	80	7	93	20.07 ± 0.03	4.5 ± 0.2	4.4 ± 0.2
165	60	6	94	19.82 ± 0.04	5.9 ± 0.2	4.1 ± 0.2

Table S2. Comparison of polymer-based dielectric materials, including dielectric constant (ε_r) and dielectric loss (tan δ) measured at low electric field at 1 kHz, and breakdown strength (E_b), discharged energy density (U_e), charge-discharge efficiency (η) measured at high electric field.

Material	ε_r	tan δ	E_b (kV mm^{-1})	U_e (J cm^{-3})	η (%)	Ref.
Linear dielectrics						
Biaxially-oriented polypropylene (BOPP)	2.3	0.0002	650	4	83	3
Polypropylene (PP)	2.2	0.0002	600	3.6	80	4
Polycarbonate (PC)	3.0	0.002	650	5	40	5
Polyetherimide (PEI)	3.2	0.003	500	3	N.A.	6
Polyphenylene oxide (PPO)	2.8	0.001	900	0.9	85	3
Dipolar glass dielectrics						
Polyimide (PI)	3.2	0.01	450	5.2	90	7
Aromatic Polythiourea (ArPTU)	4.4	0.01	1000	22	92	8
Poly(ether-ester-urethane) (PEEU)	4.7	0.015	600	8	90	9
Sulfonylated Polymer of Intrinsic Microporosity (SO_2-PIM)	6.0	0.005	770	17	90	10
Sulfonylated Poly (ether ether ketone) (PEEK-SO_2)	5.0	0.01	300	2.35	90	11
Sulfonylated Poly (2,6-dimethyl-1,4-phenylene oxide) (SO_2-PPO_{25})	5.9	0.003	800	22	92	12
poly(2-(methylsulfonyl) ethyl methacrylate) (PMSEMA)	11.4	0.02	270	5.7	80	13
Meta-aromatic polyurea (META-PU)	5.8	0.01	670	13	91	14
PVDF-based pure polymers						
PVDF	12	0.05	600	12.5	56	15
PVDF strehced (500 % strain)	12	0.05	800	27.1	68	16
PVDF-CTFE	13	0.03	600	25	N.A.	17
PVDF-HFP	10	0.03	600	13.5	55	18
PVDF-HFP stretched (500 % strain)	12	0.05	900	27.7	65	16
PVDF-HFP stretched (800 % strain)	13	0.04	660	20	71	19

PVDF-TRFE-CTFE	60	0.1	500	13	60	[20]
PVDF-TRFE-CFE	53	0.07	490	11.3	52	[15]
PTFE-HFP-VDF	6	0.01	600	6	95	[21]
PVDF-based polymer blends						
PVDF-TRFE-CFE/PVDF	29	0.05	640	19.6	60	[15]
P(VDF-HFP)/P(VDF-TrFE-CFE) multilayers	16	N.A.	600	20	85	[22]
PVDF-HFP/PVDF-TrFE-CTFE	29	0.06	600	21.9	63	[23]
PVDF-HFP/PMMA/PC	4.7	0.02	600	8.4	60	[24]
PVDF/PC	4.5	0.01	800	15	N.A.	[25]
PVDF-HFP/PET/PMMA	5	0.01	800	17.4	N.A.	[26]
PVDF-TRFE-CTFE/ArPTU	11.3	0.01	700	19.2	85	[27]
PVDF-HFP/PMMA	6.5	0.025	475	11.2	85	[28]
PVDF-HFP/PC multilayer	3	0.005	460	N.A.	90	[29]
PVDF-HFP/PC blends 10/90	3.5	0.005	500	N.A.	87	[29]
PVDF-based nanocomposites						
PVDF-HFP/$BaTiO_3$@TiO_2_nanofibre	20	0.04	800	31.2	78	[30]
PVDF-HFP/$BaTiO_3$_nanoparticle	11	0.05	650	20.6	74	[31]
PVDF/$BaTiO_3$_nanoparticle/Titanite coupling agent	12	0.04	517	11.2	62	[32]
PVDF/$Ba_{0.2}Sr_{0.8}TiO_3$_nanowire	17.5	N.A.	450	14.8	61	[33]
PVDF/$BaTiO_3$@sheet-likeTiO_2	21	0.05	490	17.6	N.A.	[34]
PVDF/$BaTiO_3$ sandwich structure	17	0.04	470	18.8	65	[35]
PVDF/$BaTiO_3$ sandwich structure	11	0.04	410	16.2	70	[36]
PVDF-HFP/$BaTiO_3$ sandwich structure	11.5	0.04	526	26.4	72	[37]
PVDF-TRFE-CFE/Boron Nitride Nanosheet (BNNS)	38	0.03	650	22.3	77	[38]
PVDF/$CaNbO_3$	10.5	N.A.	792	36	61	[39]

Table S3. Comparison of melting temperature (T_m), fusion enthalpy (ΔH_m), and calculated crystallinity (χ) for Roll & Press PVDF films with ΔC_h of 3 mm prepared at T_p of 60 °C and T_{max} of 165 °C, followed by annealing at 165 °C, 140 °C, 80 °C and 60 °C. Hot-pressed PVDF films were measured as references. All data were collected during the first heating process.

T_{anneal}	First heating		
	T_m (°C)	ΔH_m (J/g)	χ (%)
60 °C	172.5 ± 1	39 ± 1	38 ± 1
80 °C	172.5 ± 1	38 ± 3	37 ± 3
140 °C	171.6 ± 1	41 ± 2	39 ± 2
165 °C	172.3 ± 1	46 ± 2	44 ± 2
Hot-pressed	172.5 ± 1	48 ± 2	46 ± 2

Reference

1. X. Ren, N. Meng, H. Zhang, J. Wu, I. Abrahams, H. Yan, E. Bilotti and M. J. Reece, *Nano Energy*, 2020, **72**, 104662.
2. N. Meng, X. Ren, G. Santagiuliana, L. Ventura, H. Zhang, J. Wu, H. Yan, M. J. Reece and E. Bilotti, *Nature Communications*, 2019, **10**, 4535.
3. Q. Chen, Y. Wang, X. Zhou, Q. M. Zhang and S. Zhang, *Appl. Phys. Lett.*, 2008, **92**, 142909.
4. G. Zhang, D. Brannum, D. Dong, L. Tang, E. Allahyarov, S. Tang, K. Kodweis, J.-K. Lee and L. Zhu, *Chem. Mater.*, 2016, **28**, 4646-4660.
5. Q. Li, L. Chen, M. R. Gadinski, S. Zhang, G. Zhang, H. U. Li, E. Iagodkine, A. Haque, L.-Q. Chen, T. N. Jackson and Q. Wang, *Nature*, 2015, **523**, 576-579.
6. J. Ho and R. Jow, *Characterization of high temperature polymer thin films for power conditioning capacitors*, ARMY RESEARCH LAB ADELPHI MD SENSORS AND ELECTRON DEVICES DIRECTORATE, 2009.
7. P. Hu, W. Sun, M. Fan, J. Qian, J. Jiang, Z. Dan, Y. Lin, C.-W. Nan, M. Li and Y. Shen, *Appl. Surf. Sci.*, 2018, **458**, 743-750.
8. S. Wu, W. Li, M. Lin, Q. Burlingame, Q. Chen, A. Payzant, K. Xiao and Q. M. Zhang, *Adv. Mater.*, 2013, **25**, 1734-1738.
9. T. Zhang, X. Chen, Y. Thakur, B. Lu, Q. Zhang, J. Runt and Q. M. Zhang, *Science Advances*, 2020, **6**, eaax6622.
10. Z. Zhang, J. Zheng, K. Premasiri, M.-H. Kwok, Q. Li, R. Li, S. Zhang, M. H. Litt, X. P. A. Gao and L. Zhu, *Materials Horizons*, 2020, **7**, 592-597.
11. J. Wei, T. Ju, W. Huang, J. Song, N. Yan, F. Wang, A. Shen, Z. Li and L. Zhu, *Polymer*, 2019, **178**, 121688.
12. Z. Zhang, D. H. Wang, M. H. Litt, L. S. Tan and L. Zhu, *Angew. Chem.*, 2018, **130**, 1544-1547.
13. J. Wei, Z. Zhang, J.-K. Tseng, I. Treufeld, X. Liu, M. H. Litt and L. Zhu, *ACS Appl. Mater. Interfaces*, 2015, **7**, 5248-5257.
14. S. Wu, M. Lin, Q. Burlingame and Q. M. Zhang, *Appl. Phys. Lett.*, 2014, **104**, 072903.
15. X. Zhang, Y. Shen, Z. Shen, J. Jiang, L. Chen and C.-W. Nan, *ACS Appl. Mater. Interfaces*, 2016, **8**, 27236-27242.
16. W. Xia, Z. Zhou, Y. Liu, Q. Wang and Z. Zhang, *J. Appl. Polym. Sci.*, 2018, **135**, 46306.
17. X. Zhou, B. Chu, B. Neese, M. Lin and Q. M. Zhang, *ITDEI*, 2007, **14**, 1133-1138.
18. F. Guan, J. Pan, J. Wang, Q. Wang and L. Zhu, *Macromolecules*, 2010, **43**, 384-392.
19. M. Yuan, B. Li, S. Zhang, R. Rajagopalan and M. T. Lanagan, *ACS Applied Polymer Materials*, 2020, **2**, 1356-1368.
20. Z. Zhang and T. C. M. Chung, *Macromolecules*, 2007, **40**, 783-785.
21. S. Zhang, C. Zou, D. I. Kushner, X. Zhou, R. J. Orchard, N. Zhang and Q. M. Zhang, *ITDEI*, 2012, **19**, 1158-1166.
22. J. Jiang, Z. Shen, J. Qian, Z. Dan, M. Guo, Y. Lin, C.-W. Nan, L. Chen and Y. Shen, *Energy Storage Materials*, 2019, **18**, 213-221.
23. X. Ren, N. Meng, H. Yan, E. Bilotti and M. J. Reece, *Polymer*, 2019, **168**, 246-254.
24. Z. Zhou, J. Carr, M. Mackey, K. Yin, D. Schuele, L. Zhu and E. Baer, *J. Polym. Sci., Part B: Polym. Phys.*, 2013, **51**, 978-991.
25. X. Chen, J.-K. Tseng, I. Treufeld, M. Mackey, D. E. Schuele, R. Li, M. Fukuto, E. Baer and L. Zhu, *J. Mater. Chem. C*, 2017, **5**, 10417-10426.

26. K. Yin, Z. Zhou, D. E. Schuele, M. Wolak, L. Zhu and E. Baer, *ACS Appl. Mater. Interfaces*, 2016, **8**, 13555-13566.
27. H. Zhu, Z. Liu and F. Wang, *JMatS*, 2017, **52**, 5048-5059.
28. B. Luo, X. Wang, H. Wang, Z. Cai and L. Li, *Composites Sci. Technol.*, 2017, **151**, 94-103.
29. J.-K. Tseng, K. Yin, Z. Zhang, M. Mackey, E. Baer and L. Zhu, *Polymer*, 2019, **172**, 221-230.
30. X. Zhang, Y. Shen, B. Xu, Q. Zhang, L. Gu, J. Jiang, J. Ma, Y. Lin and C.-W. Nan, *Adv. Mater.*, 2016, **28**, 2055-2061.
31. J. Jiang, X. Zhang, Z. Dan, J. Ma, Y. Lin, M. Li, C.-W. Nan and Y. Shen, *ACS Appl. Mater. Interfaces*, 2017, **9**, 29717-29731.
32. P. Hu, S. Gao, Y. Zhang, L. Zhang and C. Wang, *Composites Sci. Technol.*, 2018, **156**, 109-116.
33. H. Tang and H. A. Sodano, *Nano Lett.*, 2013, **13**, 1373-1379.
34. R. Su, Z. Luo, D. Zhang, Y. Liu, Z. Wang, J. Li, J. Bian, Y. Li, X. Hu, J. Gao and Y. Yang, *The Journal of Physical Chemistry C*, 2016, **120**, 11769-11776.
35. Y. Wang, J. Cui, Q. Yuan, Y. Niu, Y. Bai and H. Wang, *Adv. Mater.*, 2015, **27**, 6658-6663.
36. Y. Wang, J. Cui, L. Wang, Q. Yuan, Y. Niu, J. Chen, Q. Wang and H. Wang, *J. Mater. Chem. A*, 2017, **5**, 4710-4718.
37. Y. Wang, L. Wang, Q. Yuan, J. Chen, Y. Niu, X. Xu, Y. Cheng, B. Yao, Q. Wang and H. Wang, *Nano Energy*, 2018, **44**, 364-370.
38. Q. Li, G. Zhang, F. Liu, K. Han, M. R. Gadinski, C. Xiong and Q. Wang, *Energy & Environmental Science*, 2015, **8**, 922-931.
39. Z. Bao, C. Hou, Z. Shen, H. Sun, G. Zhang, Z. Luo, Z. Dai, C. Wang, X. Chen and L. Li, *Adv. Mater.*, 2020, 1907227.